Title
Elimination of Response to Relative Humidity Changes in Chemical-Sensitive Field-Effect Transistors

Journal
ACS Sensors, 4(7)

ISSN
2379-3694

Authors
Gupta, Niharika
Fahad, Hossain M
Amani, Matin
et al.

Publication Date
2019-07-26

DOI
10.1021/acssensors.9b00637

Peer reviewed

Elimination of Response to Relative Humidity Changes in Chemical-Sensitive Field Effect Transistors

Niharika Gupta[1,2,3], Hossain M. Fahad[1,2,3], Matin Amani[1,2,3], Xiaohui Song[4,5], Mary Scott[4,5], and Ali Javey[1,2,3]*

[1]Electrical Engineering & Computer Sciences, University of California, Berkeley, CA 94720, USA

[2]Berkeley Sensor and Actuator Center, University of California, Berkeley, CA 94720, USA

[3]Materials Sciences Division, Lawrence Berkeley National Laboratory, Berkeley, CA 94720, USA

[4]Department of Materials Science and Engineering, University of California, Berkeley, CA 94720, USA

[5]The Molecular Foundry, Lawrence Berkeley National Laboratory, Berkeley, CA 94720, USA

*Correspondence should be addressed to A.J. (ajavey@berkeley.edu)

Abstract: Detecting accurate concentrations of gas in environments with dynamically changing relative humidity conditions has been a challenge in gas sensing technology. We report a method to eliminate effects of humidity response in chemical sensitive field effect transistors using microheaters.

Using hydrogen gas sensor with Pt/FOTS active material as a test case, we demonstrate that a sensor response of 3844% to a relative humidity change of 50% to 90% at 25 °C can be reduced to a negligible response of 11.6% by utilizing microheaters. We also show the advantage of this technique in maintaining same sensitivity in changing ambient temperatures and its application to the nitrogen dioxide gas sensors.

Keywords: gas sensors, hydrogen, humidity, microheaters, temperature dependence.

Selectivity is one of the most important figures of merit for gas sensors which includes insensitivity to ambient relative humidity and temperature changes. The sensitivity to these ubiquitous variations is currently the major limiting factor of important gas sensing applications such as air-quality monitoring[1-4] and medical diagnosis[5-7]. The fact that most of the active sensing materials interact with water makes achieving humidity insensitivity a challenge.[8-10] Chemical or gas sensor being responsive to even slightest of environmental changes leads to deviated sensor signal following inaccurate detection of gas and/or interpretation of gas concentration. Therefore, elimination of humidity and temperature is essential to having a robust and precise sensor signal.

Research in making gas sensors humidity and temperature insensitive can be divided into two strategies – computational and experimental methods. The computational method involves signal processing utilizing data from

humidity and temperature sensors along with sensor data at different concentrations in different humidity and temperature levels to calculate exact gas concentration. Multivariate calibration methods such as principal component regression (PCR)[11], partial least square (PLS)[12] and artificial neural networks (ANN)[13] have been utilized to compensate for the sensor response to humidity changes. With requirements of huge data sets needed to train the ANN and linear data sets in other methods, the computation method is also disadvantageous because of the complexity of calibration required for different combinations of relative humidity and temperature. Additionally, both of humidity and temperature sensors would need to have selective signal responses with respect to each other, which being experimentally impractical to achieve, would need further post-processing adding to the calibration complexity. Research in experimental methods include functionalization with hydrophobic materials[14] and modifications to the active sensing material either by annealing[15], doping[16, 17] or specialized growth conditions[18, 19]. These techniques decrease the sites available for water interaction, thereby reducing the response to humidity. However, the previous work studying these techniques have not been able to fully eliminate the response to humidity variations and focus on either response to gas in different humidity levels or the response to varying humidity and have not considered them as a combined problem. The dominant technology for gas sensing, metal oxide semiconductor (MOS) sensors is humidity insensitive due to high operating temperature >200 °C, boiling off any water

molecule on the active sensing part but is disadvantageous due to power consumption and safety issues at these high temperatures for applications in consumer electronics.

In this work, we demonstrate a simple technique to eliminate sensor response to variations to relative humidity in chemical-sensitive field effect transistors (CS-FETs) using microheaters. CS-FETs are nanoscale silicon transistors with the exception that the electrical gate replaced by a chemical sensing layer consisting of nanoparticles. The work-function and/or morphology of the sensing layer changes upon exposure to target chemical species, resulting in strong output drain current modulation enabling high detection sensitivity. The relevant details about the device and sensing characteristics have been explained in our previous work[20] with fabrication details in Supplementary Information S1. In the past, we utilized the microheaters by pulsing them immediately after the detection of target gas, which resulted in dramatically improved recovery times[21]. Compared to our previous work on bulk silicon CS-FETs, the distinguishing feature here is the integration of local on-chip microheaters around the sensors as shown in Fig. 1a (schematic of cross-section in Fig. 1b). As a “litmus” test to prove this technique, active sensing layer of platinum nanoparticles on trichloro(1H,1H,2H,2H-perfluorooctyl) silane (FOTS) was chosen. The top-down image of the Pt/FOTS layer on SiO_2 grids is shown in Fig. 1c. This layer can be used for the detection of hydrogen gas; reason being the strong interaction between Pt and hydrogen gas[22], and enhanced sensor

performance characteristics with FOTS underneath Pt (Supplementary Information S2). Even though this can enable detection of hydrogen in ppm levels, it's highly sensitive to relative humidity change which made it the best candidate to prove this technique.

Results and discussion

The method to achieve negligible cross-sensitivity to relative humidity change with the CS-FET platform is to operate the microheaters in a constant voltage mode such that the chip is at a slightly elevated temperature level above room temperature. Infrared imaging of the chip under different microheater powers between zero and 560 mW suggested that the chip temperature increased linearly with power, shown in Supplementary Information S3 (infrared images in Supplementary Information S4). For a relative humidity change from 50% to 90% with a drain bias of 0.8 V, the CS-FET manifested a response of 3844%, as depicted in Fig. 2a. Sensor response were calculated as percentage change from the baseline current values $(I_{peak} - I_{baseline})/I_{baseline}) \times 100$. The ambient temperature of the sensor was regulated at 25 °C and since relative humidity level was not increased beyond 95%, the chip was operated above the dew point for condensation to occur. However, the plot of sensor response *vs* humidity (Supplementary Information S5) extracted from Fig. 2a, revealed hysteresis in the adsorption and desorption curves at room temperature, a signature of capillary condensation.[23] A schematic of the occurrence of the phenomenon on the nanoparticles is shown in Fig. 1d. From our previous work[21], the examination

of cross-section using transmission electron microscopy (TEM) revealed that the thickness of the nanoparticles should be between 3-4 nm for Au_{1nm}-$Pd_{0.3nm}$. Since this material system was deposited using the same technique as Pt_{1nm} with the same conditions, similar range of height for Pt nanoparticles is expected. However, to find the approximate relative humidity level at which capillary condensation will occur at room temperature, it was assumed that the size of the nanoparticles is much larger than the cavity size (this might underestimate the actual level for onset according to literature where it has been shown that as the radius of curvature of the nanoparticles increases, the water meniscus height calculated using Monte Carlo simulations also increases for the same relative humidity level[24]). The cavity size between most of the nanoparticles was found out to be 2 nm from Fig. 1c. Even though the validity of the Kelvin equation for sub-10 nm has been debatable, it was assumed valid for a rough approximation of the relative humidity level that creates onset of capillary condensation. The following approximate form of the Kelvin equation[25] was applied:

$$\frac{p_{sat}}{p_v} = \exp\left(\frac{2\gamma V_m cos\Theta}{dRT}\right) \quad (1)$$

where p_{sat} is the saturated vapor pressure, p_v is the vapor pressure, γ is the water surface tension, V_m is the molar volume of water, Θ is the contact angle of water with the nanoparticle surface, d is the diameter of the capillary, R is the universal gas constant, and T is the temperature.[26, 27] Given

that pure water completely wets contaminants-free platinum[28], it was assumed that the platinum nanoparticles were pure in quality and exhibited zero contact angle with water. Utilizing the standard values of water surface tension as 72 dynes/cm and molar volume of 18 cm^3 at room temperature, the value of relative pressure, p_v/p_{sat} which is equivalent to relative humidity, was calculated to be 59%, indicating condensation between the cavities formed in the nanoparticle assembly below the dew point pressure.

However, with increasing microheater power, the sensor response to this relative humidity change decreased exponentially (Fig. 2b), with negligible sensor response of 11.6% at a power of 372 mW and corresponding chip temperature of 37 ± 3 °C. The rationale behind this is the increase in evaporation rate of any condensed water as the surface temperature is increased. Additionally, physisorption rate of water molecules on the sensing material decreases with increasing chip temperature (which can be explained by Le Chatelier's principle[29]), given adsorption is an exothermic reaction. For the same reason, the overall hydrogen response also decreased with increasing chip temperature (Supplementary Information S6), but this came at the benefit of eliminated humidity response. The reason for the relatively low chip temperatures (below <100 °C) requirement to eliminate response to humidity is the fact that water can be evaporated instead of being boiled-off, also the high surface-to-volume ratio of nanoparticles allow for high evaporation rate unlike the active 'thick' films in MOS sensors and other gas sensors based on field effect transistors. As a side note, the high

surface-to-volume ratio of the nanoparticles is also one of the reasons for high sensitivity to humidity providing the large number of active sites for water adsorption, but if the size of nanoparticles is decreased to circumvent the problem, the sensitivity to hydrogen will also be lowered.

Additionally, we observed minor reductions in sensitivity to hydrogen in relative humidity levels of 50% and 90% with sensor response being 490% (250 ppm) and 1488% (1000 ppm), and 464% (250 ppm) and 1539% (1000 ppm), respectively, as shown in Fig 2c. This measurement was carried out with a different CS-FET sensor with 0.65 V of drain bias (to match the baseline current with the CS-FET with 0.8 V drain bias) for which chip temperature to eliminate humidity response was 64 ± 8 °C. The concentrations of 250 ppm and 1000 ppm of hydrogen were chosen for these tests because of the linear sensor characteristics observed between 100 ppm and 1000 ppm (Fig. 3a and 3b), enabling us to hypothesize that the sensitivity (sensor response per ppm) is constant between those concentration levels. Measurements in Fig. 3a were performed with chip temperature of 37 ± 3 °C to eliminate the response to humidity change. The trends of response (t_{90}) and recovery (t_{10}) times with varying hydrogen concentration are depicted in Fig. 3c and 3d respectively. t_{90} is the time taken for the sensor to reach 90% of its peak response value from the baseline current and t_{10} is the time taken for the sensor to recover to 10% of its baseline current from the peak value. Fig. 3e shows that the sensor proved to be highly selective against other gases such as methane, carbon

dioxide, ammonia, nitrogen dioxide and sulfur dioxide, though not against hydrogen sulfide. Even though the molecular structure of water and H_2S is the same, the CS-FET at elevated temperature is sensitive to the gas while not being to water because of the stronger interaction between the active material and the gas, also making H_2S notorious for its poisoning action to catalysts including platinum[30-34]. The CS-FET shown in Fig. 3f with microheater switched-on for ten days and chip temperature of 51 ± 6 °C exhibited negligible drift, implying that the active material and the silane layer remained intact and unaffected by continuous microheater operation. This is attributed to the operating temperature of the microheaters, which is around 10 times lower than the degradation temperature of FOTS[35] and 20 times than that of Pt[36].

Additional advantage of using the microheaters was the insignificant variation in gas sensitivity with changing ambient temperature. Three pulses of hydrogen gas with concentration of 100 ppm, 600 ppm and 1000 ppm were injected in ambient temperatures of 15 °C, 25 °C and 35 °C with a drain bias of 0.6 V and it was seen that the sensitivity decreased by around 5 times as ambient temperature was lowered by 20 °C, from 2.2%/ppm at 35 °C to 0.4%/ppm at 15 °C as shown in Fig. 1a. However, when the microheaters were kept switched-on at a power of 372 mW (chip temperature of 35 ± 3 °C), the sensitivity remained roughly constant; 1.6%/ppm at 35 °C, 1.7%/ppm at 25 °C and 1.8%/ppm at 15 °C, as demonstrated in Fig. 4b (raw data is shown in Supplementary information

S7). The benefit of maintaining the constant sensitivity regardless of the ambient temperature dramatically simplifies calibration process and ensure detection of low concentration levels as the ambient temperature lowers, for practical usage.

In addition to demonstrating humidity selective hydrogen detection using the Pt/FOTS system, we show this technique's application to active sensing materials for other gases with the CS-FET platform. Fig. 5a demonstrates that the CS-FET with drain bias as 4 V and InO_x thin film (~1.5 nm) as active material responded by 895% to relative humidity change from 50% to 90%. With microheaters turned on to keep the chip temperature at 70 ± 8 °C, the sensor showed negligible sensor response to the humidity change along with constant sensor response, -56% and -52% to 100 ppb NO_2 in the humidity levels of 50% and 90% respectively (Fig. 5b).

Conclusion

In conclusion, we have demonstrated that by keeping the temperature of the CS-FET slightly higher than the ambient temperature by utilizing the microheaters, effects of relative humidity change can be eliminated. Added benefits of constant gas sensitivity using this technique in different ambient temperatures have also been proved. We showed the proof-of-concept for this technique using Pt/FOTS as active material for hydrogen sensing and its application to InO_x for nitrogen dioxide sensing.

The microheater material and design will be optimized in our future work and it is expected that the power needed to reach the chip temperature levels to eliminate humidity response will be much lower, extending the applicability of this technique for gas sensors in consumer electronics. Temperature sensor will be also fabricated on the same chip so that the heaters can be looped with proportional-integral-derivative (PID) controller to maintain constant chip temperature irrespective of ambient temperature for constant sensor responses to same gas concentration level.

Though the employability of this technique with other material systems, specifically their long-term sustainability to the heat emitted by microheaters remains a question now, as the library of gases detected with CS-FET platform expands, the method provides a good beginning to solve the long-standing problem of humidity response in gas sensors based on field-effect transistors.

METHODS

Measurement Apparatus

CS-FET device chips were wire bonded to a 84-pin J-bend leaded chip carrier. Pure dry air was used as diluent gas and was procured from Praxair Technology Inc. For H_2 (Fig. 2-4) and NO_2 (Fig. 5) sensing experiments, 1% H_2 in N_2 (Gasco) and 1 ppm NO_2 (Gasco) in N_2 were used as source respectively. Selectivity measurements in Fig. 3e were performed with 2.5% CH_4, 100 ppm CO_2, 50 ppm NH_3, 5 ppm NO_2, 50 ppm SO_2 and 50 ppm H_2S in

N_2 (Mesa gas) as sources. Typical gas flow rates were from 1 to 100 sccm, and diluent (air) flow rate was approximately 1000 sccm. Gas delivery was controlled by mass flow controllers (Alicat Scientific Inc.). Measurements involving relative humidity and temperature changes were done in ESPEC Humidity and Temperature Cabinet LHU-113 with gas outlet 1-2 cm from the sensor chip, otherwise in a walk-in fumehood. CS-FET sensors were biased using a Keithley 428 current preamplifier, and the current signals were acquired using a LabVIEW-controlled data acquisition unit (National Instruments, NI USB-6211). The microheaters were powered by the Agilent E3631A DC Power Supply and all the measurements were performed with microheaters placed on the adjacent die to the one with the CS-FET. Infrared images in Supplementary figure S3 were taken using FLIR ETS320.

Fabrication process

A schematic representing the fabrication process is depicted in Supporting Information S1. CS-FET gas sensors were fabricated on prime grade silicon ⟨100⟩ wafers with sheet resistivity in the range of 10–20 Ω·cm. Before processing, all wafers were cleaned in a standard piranha (1:4, hydrogen peroxide/sulfuric acid) bath at 120 °C and native oxide was removed using a 10 s dip in 1:10 hydrofluoric acid. First, a 350 nm silicon dioxide was thermally grown on the silicon wafers for device isolation, using a three-step dry (5 min)–wet (55 min)–dry (5 min) oxidation process at 1000 °C, at atmospheric pressure for 55 min. Oxide thickness was verified using fixed angle ellipsometry. Next, source and drain doping regions in silicon were

defined using a standard i-line photolithography process (Fujifilm, photoresist: OiR 906-12, developer: OPD-4262) and wet etching the isolation oxide (in 5:1 buffered hydrofluoric acid for 5 min). Following this, ion implantation ($4.5e^{14}$ cm^{-2}, Phosphorus, 15 KeV) was performed for source-drain doping. To complete the formation of n+2 doped regions, phosphorus drive-in and activation was performed in the silicon source and drain by rapid thermal annealing (RTA) at 1050 °C for 30 s in N_2. The “gate” or sensing layer region was patterned next and etched in 5:1 buffered hydrofluoric acid for 4 min. The channel doping was also performed using ion implantation ($5e^{11}$ cm^{-2}, Phosphorus, 18 KeV) and subsequently rapid thermal annealing (RTA) at 900 ℃ for 1 s in N_2. To define source and drain contacts, a separate source-drain metallization mask was used, which underlaps the doped source and drain regions by 11 µm. After this, argon was sputtered to etch the native oxide and then, 20 nm of nickel and 50 nm tungsten were then deposited in the source and drain contact regions, also using the sputtering tool followed by lift-off in acetone. To achieve ohmic source and drain contacts, nickel silicidation (NiSi) was performed in forming gas (5% H_2 in N_2) using RTA at 400 °C for 5 min. To pattern the microheaters, photolithography was performed and consecutively, 200 nm tungsten was sputtered. The fabrication of bare CS-FET concluded with lift-off.

For the hydrogen sensor, FOTS was deposited using AMST Molecular Vapor Deposition MVD100. Following this, Pt sensing layer was deposited by electron beam evaporation of 1 nm Pt. For the nitrogen oxide sensor, InO_x

sensing layer was deposited by thermal evaporation of 1.5 nm InO_x after which the chip was annealed in forming gas at 150 °C for 1 h postdeposition, which completed the sensor fabrication process.

References:

1. Wei, P.; Ning, Z.; Ye, S.; Sun, L.; Yang, F.; Wong, K. C.; Westerdahl, D.; Louie, P. K. K. Impact Analysis of Temperature and Humidity Conditions on Electrochemical Sensor Response in Ambient Air Quality Monitoring. *Sensors (Basel)*. **2018**, *18* (2), 59, DOI: 10.3390/s18020059
2. Fang, L.; Clausen, G.; Fanger, O. P. Impact of Temperature and Humidity on the Perception of Indoor Air Quality. *Indoor Air*. **1998**, *8*, 80-90, DOI: 10.1111/j.1600-0668.1998.t01-2-00003.x
3. Pang, X.; Shaw, S. D.; Gillot, S.; Lewis, A. C. The Impacts of Water Vapour and Co-pollutants on the Performance of Electrochemical Gas Sensors Used for Air Quality Monitoring. *Sensors and Actuators B: Chemical*. **2018**, *266*, 674-684, DOI: 10.1016/j.snb.2018.03.144
4. Spicer, C. W.; Joseph, D. W.; Ollison, W. M. A Re-Examination of Ambient Air Ozone Monitor Interferences. *Journal of the Air & Waste Management Association*. **2012**, *60* (11), 1353-1364, DOI: 10.3155/1047-3289.60.11.1353
5. Ong, K.G.; Zeng, K.; Grimes, C.A. A Wireless, Passive Carbon Nanotube-Based Gas Sensor. *IEEE Sensors Journal*. **2002**, 2 (2), 82-88, DOI: 10.1109/JSEN.2002.1000247
6. Huang, H.; Zhou, J.; Chen, S.; Zeng, L.; Huang, Y. A Highly Sensitive QCM Sensor Coated with Ag+-ZSM-5 Film for Medical Diagnosis. *Sensors and Actuators B: Chemical*. **2004**, *101* (3), 316-321, DOI: 10.1016/j.snb.2004.04.001

7. Montuschi, P.; Mores, N.; Trové, A.; Mondino, C.; Barnes, P.J. The Electronic Nose in Respiratory Medicine. *Respiration*. **2013**, *85*, 72–84, DOI: 10.1159/000340044
8. Boyle, J.F.; Jones, K.A. The Effects of CO, Water Vapor and Surface Temperature on the Conductivity of a SnO_2 Gas Sensor. *Journal of Electronic Materials*. **1977**, *6* (6), 717-733, DOI: 10.1007/BF02660346
9. Zhao, Z.; Knight, M.; Kumar, S.; Eisenbraun, E.T.; Carpenter, M.A. Humidity Effects on Pd/Au-Based All-Optical Hydrogen Sensors. *Sensors and Actuators B: Chemical*. **2008**, *129* (2), 726-733, DOI: 10.1016/j.snb.2007.09.032
10. Zhang, Y.; Yu, K.; Jiang, D.; Zhu, Z.; Geng, H.; Luo, L. Zinc Oxide Nanorod and Nanowire for Humidity Sensor. *Applied Surface Science*. **2005**, *242* (1–2), 212-217, DOI: 10.1016/j.apsusc.2004.08.013
11. Park, J.; Zellers, E.T.; Temperature and Humidity Compensation in the Determination of Solvent Vapors with a Microsensor System. *Analyst*. **2000**, *125*, 1775-1782, DOI: 10.1039/b004528o
12. Sohn, J.H.; Atzeni, M.; Zeller, L.; Pioggia, G. Characterization of Humidity Dependence of a Metal Oxide Semiconductor Sensor Array using Partial Least Squares. *Sensors and Actuators B: Chemical*. **2008**, *131* (1), 230-235, DOI: 10.1016/j.snb.2007.11.009
13. Mumyakmaz, B.; Özmen, A.; Ebeoğlu, M.A.; Taşaltın, C.; Gürol, İ. A Study on the Development of a Compensation Method for Humidity Effect in

QCM Sensor Responses. *Sensors and Actuators B: Chemical*. **2010**, *147* (1), 277-282, DOI: 10.1016/j.snb.2010.03.019

14. Some, S.; Xu, Y.; Kim, Y.; Yoon, Y.; Qin, H.; Kulkarni, A.; Kim, T.; Lee, H. Highly Sensitive and Selective Gas Sensor using Hydrophilic and Hydrophobic Graphenes. *Scientific Reports*. **2013**, *3* (1868), DOI: 10.1038/srep01868

15. Vasiliev, A. A.; Varfolomeev, A. E.; Volkov, I. A.; Simonenko, N. P.; Arsenov, P. V.; Vlasov, I. S.; Ivanov, V. V.; Pislyakov, A. V.; Lagutin, A. S.; Jahatspanian, I. E.; Maeder, T. Reducing Humidity Response of Gas Sensors for Medical Applications: Use of Spark Discharge Synthesis of Metal Oxide Nanoparticles. *Sensors (Basel)*. **2018**, *18* (8), 2600, DOI: 10.3390/s18082600

16. Kim, H.; Haensch, A.; Kim, I.; Barsan, N.; Weimar, U.; Lee, J. The Role of NiO Doping in Reducing the Impact of Humidity on the Performance of SnO2-Based Gas Sensors: Synthesis Strategies, and Phenomenological and Spectroscopic Studies. *Adv. Funct. Mater*. **2011**, *21*, 4456-4463, DOI: 10.1002/adfm.201101154

17. Zhang, T.; Mubeen, S.; Yoo, B.; Myung, N.V.; Deshusses, M.A. A Gas Nanosensor Unaffected by Humidity. *Nanotechnology*. **2009**, *20* (25), DOI: 10.1088/0957-4484/20/25/255501

18. Pan, X.; Zhao, X.; Bermak, A.; Fan, Z. A Humidity-Insensitive NO_2 Gas Sensor with High Selectivity. *IEEE Electron Device Letters*. **2016**, *37* (1), 92-95, DOI: 10.1109/LED.2015.2504260

19. Liu, Y.; Yao, S.; Yang, Q.; Sun, P.; Gao, Y.; Liang, X.; Liu, F.; Lu, G. Highly Sensitive and Humidity-Independent Ethanol Sensors Based on In_2O_3 Nanoflower/SnO_2 Nanoparticle Composites. *RSC Adv*. **2015**, *5*, 52252, DOI: 10.1039/c5ra07213a

20. Fahad, H. M.; Gupta, N.; Han, R.; Desai, S. B.; Javey, A. Highly Sensitive Bulk Silicon Chemical Sensors with Sub-5 nm Thin Charge Inversion Layers. *ACS Nano*. **2018**, *12* (3), 2948-2954, DOI: 10.1021/acsnano.8b00580

21. Fahad, H. M.; Shiraki, H.; Amani, M.; Zhang, C.; Hebbar, V. S.; Gao, W.; Ota, H.; Hettick, M.; Kiriya, D.; Chen, Y. -Z.; Chueh, Y. -L.; Javey, A. Room Temperature Multiplexed Gas Sensing using Chemical-Sensitive 3.5-nm-thin Silicon Transistors. *Science Advances*. **2017**, *3* (3), e1602557, DOI: 10.1126/sciadv.1602557

22. Salomonsson, A.; Eriksson, M.; Dannetun, H. Hydrogen Interaction with Platinum and Palladium Metal–Insulator–Semiconductor devices. *Journal of Applied Physics*. **2005**, *98* (1), 014505, DOI: 10.1063/1.1953866

23. Sing, K. S. W. Reporting Physisorption Data for Gas/Solid Systems. *Pure & Appl. Chem (IUPAC)*. **1982**, *54* (11), 2201-2218, DOI: 10.1515/iupac.57.0007

24. Ehrman, S. H. and Kim, S. Grand Canonical Monte Carlo Simulation Study of Capillary Condensation between Nanoparticles. *J. Chem. Phys*. **2007**, *127* (13), 134702, DOI: 10.1063/1.2786087

25. Thomson, W. On the Equilibrium of Vapour at a Curved Surface of Liquid. *Philosophical Magazine*. **1871**, *42* (282): 448–452, DOI: 10.1080/14786447108640606

26. Helmholtz, R. V. Untersuchungen über Dämpfe und Nebel, besonders über solche von Lösungen (Investigations of Vapors and Mists, and Especially of Such Things from Solutions). *Annalen der Physik*. **1886**, *263* (4), 508-543.

27. Charlaix, E. and Ciccotti, M. Capillary Condensation in Confined Media. In *Handbook of Nanophysics*; Sattler, K., Ed.; CRC Press: Boca Raton, FL, in press, **2010**; *2*.

28. Zisman W. A. and Bewig, K. W. The Wetting of Gold and Platinum by Water. *The Journal of Physical Chemistry.* **1965,** *69* (12), 4238-4242, DOI: 10.1021/j100782a029

29. Chatelier, H. L. Recherches expérimentales et théoriques sur les équilibres chimiques. *Ann. Mines*. **1888**, *13*, 157−382.

30. Chin, D. -T. and Howard, P. D. Hydrogen Sulfide Poisoning of Platinum Anode in Phosphoric Acid Fuel Cell Electrolyte. *J. Electrochem. Soc*. **1986**, *133* (12), 2447-2450, DOI: 10.1149/1.2108447

31. Mohtadi, R.; Lee, W. -K.; Cowan, S.; Zee, J. W. V.; Murthy, M. Effects of Hydrogen Sulfide on the Performance of a PEMFC. *Electrochem. Solid-State Lett*. **2003**, *6* (12), A272-A274, DOI: 10.1149/1.1621831

32. Dunleavy, J. K. Sulfur as a Catalyst Poison. *Platinum Metals Rev*. **2006**, *50* (2), 110, DOI: 10.1595/147106706X111456

33. Somorjai, G. A. On the Mechanism of Sulfur Poisoning of Platinum Catalysts. *Journal of Catalysis*. **1972**, *27* (3), 453-456, DOI: 10.1016/0021-9517(72)90183-2

34. Oudar, J. Sulfur Adsorption and Poisoning of Metallic Catalysts. *Catalysis Reviews—Science and Engineering*, **1980**, *22* (2), 171-195, DOI: 10.1080/03602458008066533

35. Zhuang, Y. X.; Hansen, O.; Knieling, T.; Wang, C.; Rombach, P.; Lang, W.; Benecke, W.; Kehlenbeck, M.; Koblitz, J. Thermal Stability of Vapor Phase Deposited Self-Assembled Monolayers for MEMS Anti-Stiction. *J. Micromech. Microeng*. **2006**, *16* (11), 2259-2264, DOI: 10.1088/0960-1317/16/11/002

36. Firebaugh, S. L.; Jensen, K. F.; Schimdt, M. A. Investigation of High-Temperature Degradation of Platinum Thin Films with an In-Situ Resistance Measurement Apparatus*. J. Microelectromechanical Systems*. **1998**, *7* (1), 128-135, DOI: 10.1109/84.661395

Author contributions: A.J. conceived the idea and supervised the project. N.G. carried out the measurements and analysis. H.M.F fabricated the CS-FET sensors. M.A. contributed to building the measurement setup. X.S. and M.S.

did the TEM characterization of the Pt/FOTS sensing layer. All authors discussed the results and wrote the paper.

Notes: H.M.F and A.J. declare competing financial interests in equity on shares of Serinus Labs, Inc. An invention disclosure on this work has been filed with the University of California, Berkeley.

Supporting information: The Supporting Information is available free of charge.

Bulk CS-FET fabrication process. Enhanced H_2 sensor response characteristics using FOTS underneath Pt (*vs* only Pt). Plot of chip temperature *vs* microheater power. Infrared imaging at different microheater powers. Adsorption and desorption hysteresis loop. Effect of heaters on gas sensor response. Experimental data of change in current to different hydrogen concentrations in changing ambient temperatures.

Acknowledgment: A. J. acknowledges the Bakar Fellows Program in funding this research work. N.G. thanks Zhen Yuan, Chaoliang Tan, Wenbo Ji, Yingbo Zhao and Der-Hsien Lien for fruitful discussions.

Figures:

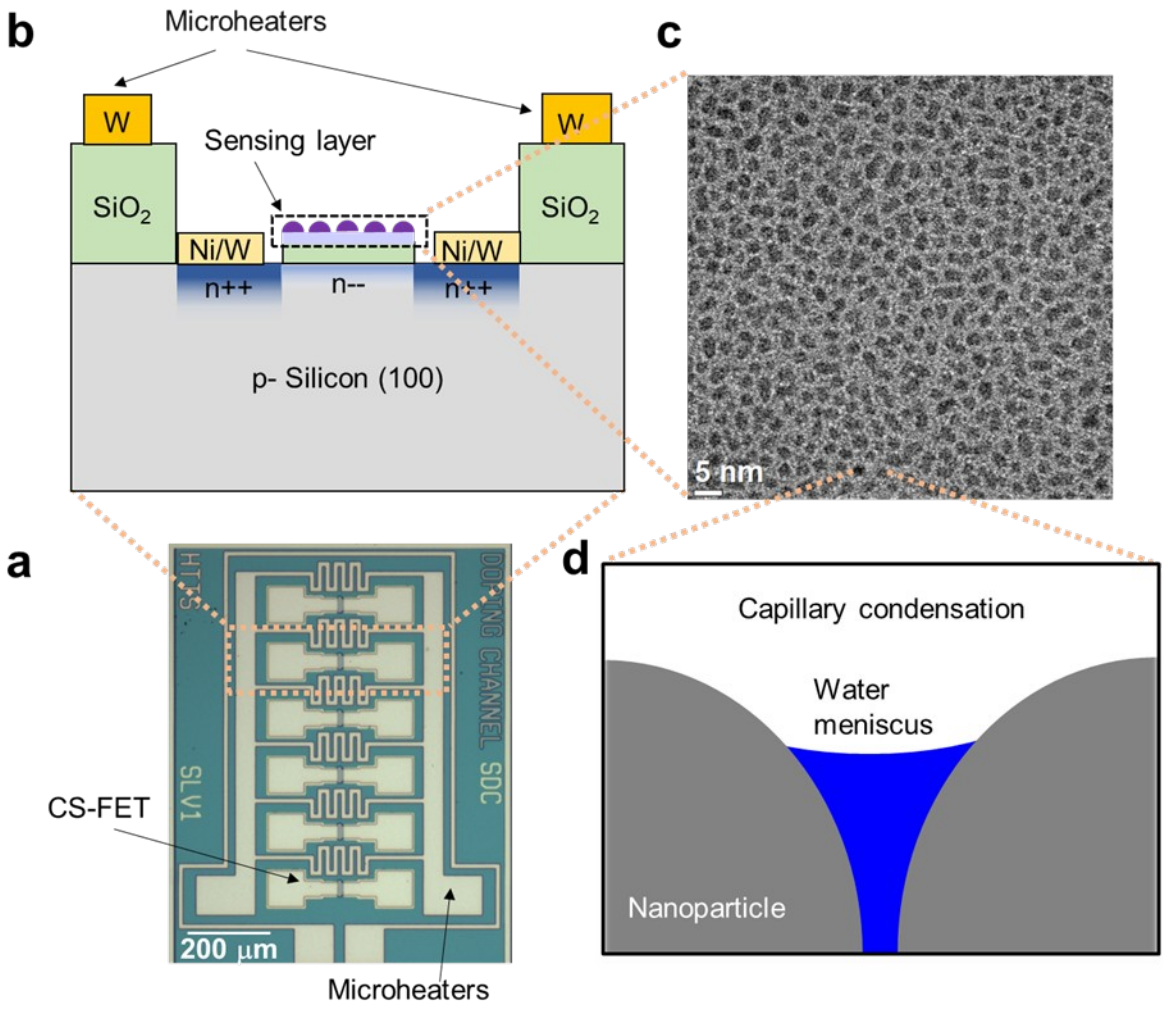

Fig. 1. (a) Optical micrograph of a competed chip showing the CS-FETs and microheaters, and a **(b)** schematic of cross-section. **(c)** Top-down transmission electron microscopic (TEM) image of Pt/FOTS on SiO_2 grids. **(d)**

Schematic of capillary condensation of water occurring in the cavity between nanoparticles.

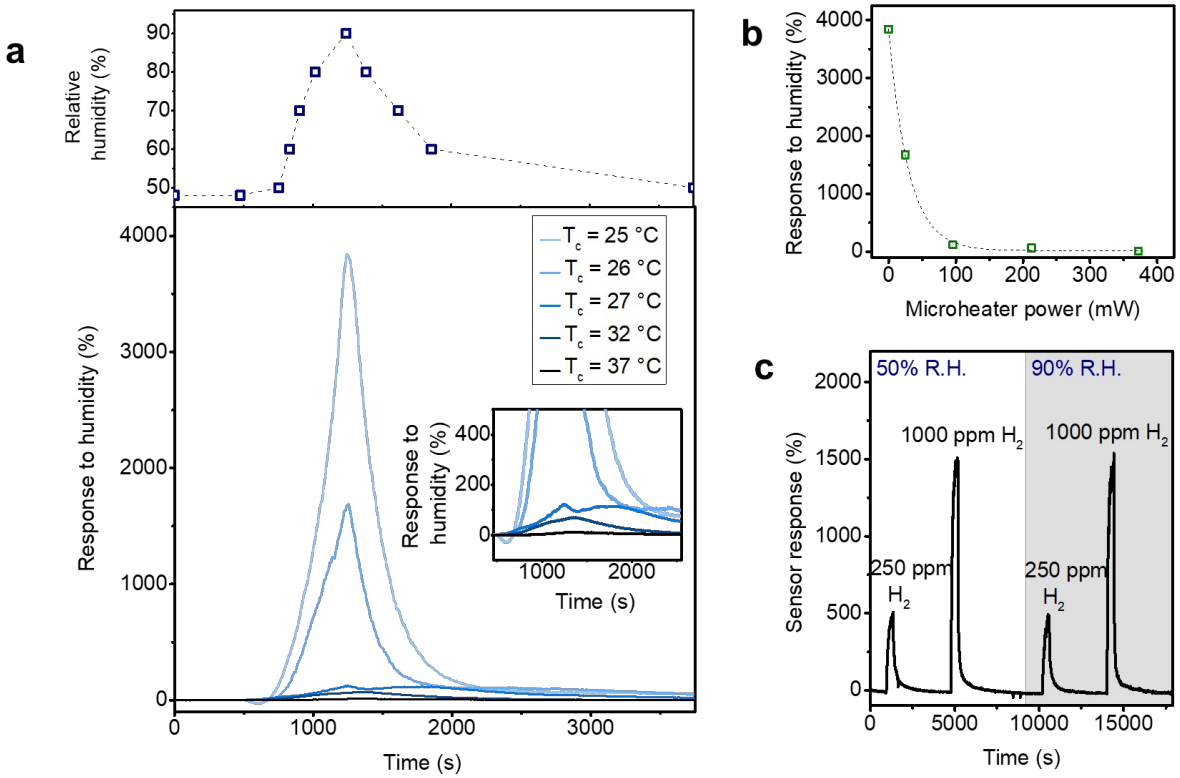

Fig. 2. (a) Sensor response to relative humidity change at 25 °C for different chip temperatures (T_c) at V_D = 0.8 V. **(b)** Sensor response to relative humidity change from 50% to 90% *vs* microheater power. **(c)** Sensor response to 250 ppm and 1000 ppm H_2 in relative humidity levels of 50% and 90% with V_D = 0.65 V, at a chip temperature of 64 ± 8 °C.

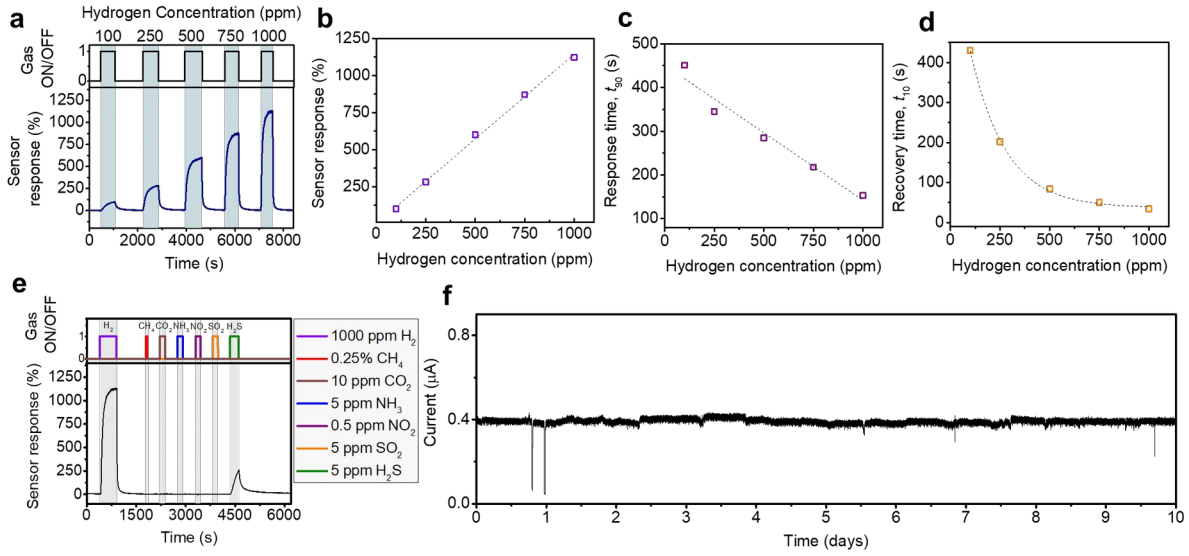

Fig. 3. (a) Sensor response *vs* time for different hydrogen concentration pulses at V_D = 0.8 V and chip temperature of 37 ± 3 °C. **(b)** Sensor response *vs* hydrogen concentration. **(c)** Response time (t_{90}) *vs* hydrogen concentration. **(d)** Recovery time (t_{10}) *vs* hydrogen concentration. **(e)** Selectivity test at V_D = 0.8 V and chip temperature of 37 ± 3 °C. **(f)** 10-day drift measurement with V_D = 0.8 V and chip temperature of 51 ± 6 °C.

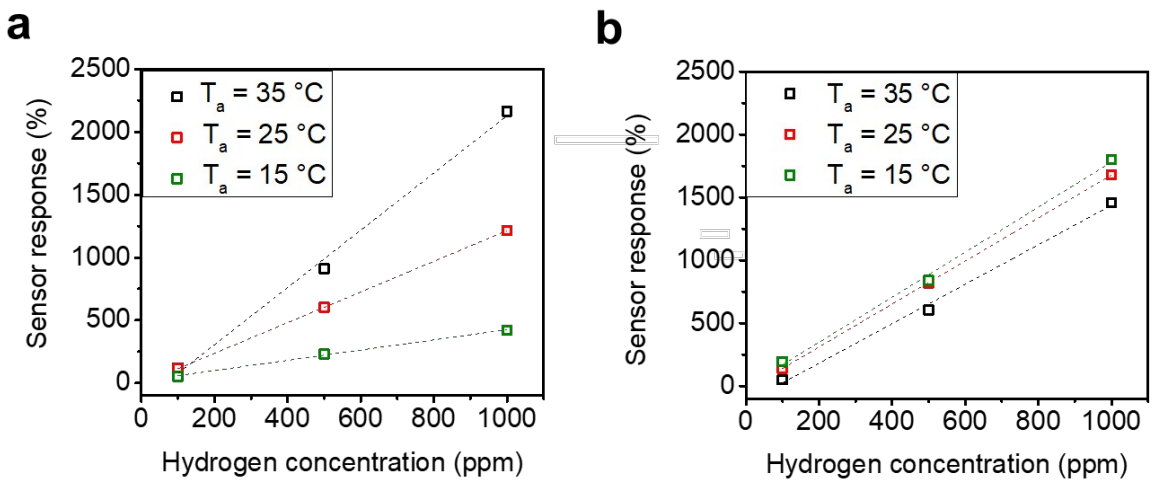

Fig. 4. Sensor response *vs* hydrogen concentration in different ambient temperatures (T_a) at V_D = 0.6 V **(a)** with microheaters off. **(b)** and with microheaters on at 372 mW.

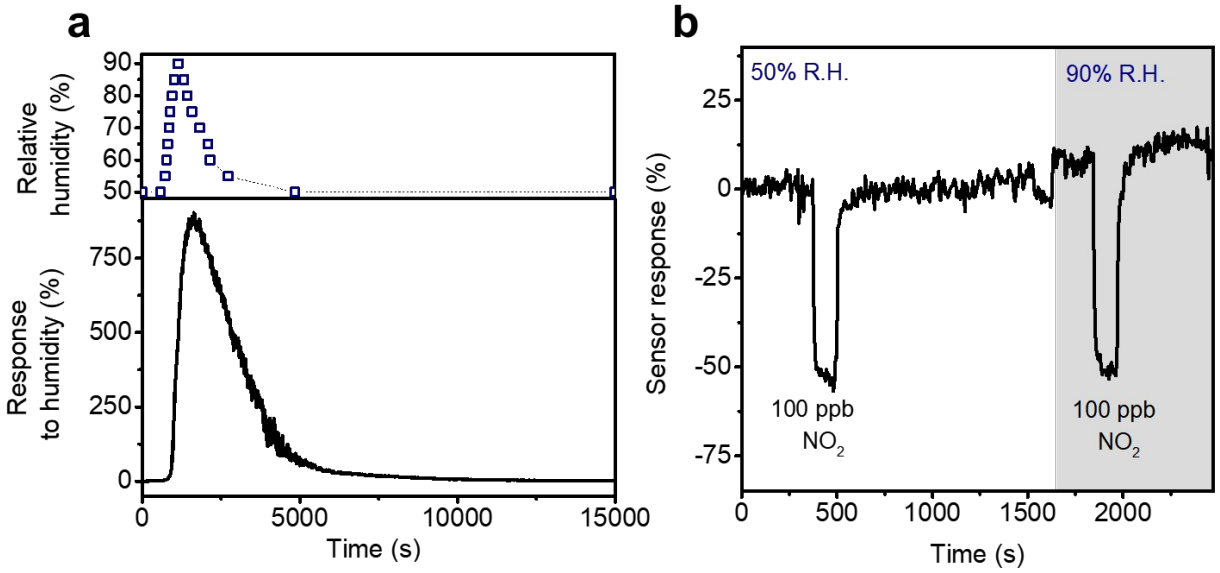

Fig. 5. (a) Sensor response to relative humidity change at 25 °C at V_D = 4 V with microheaters off. **(b)** Sensor response to 100 ppb NO_2 in relative humidity levels of 50% and 90% with microheaters on and chip temperature of 70 ± 8 °C.

TOC Figure

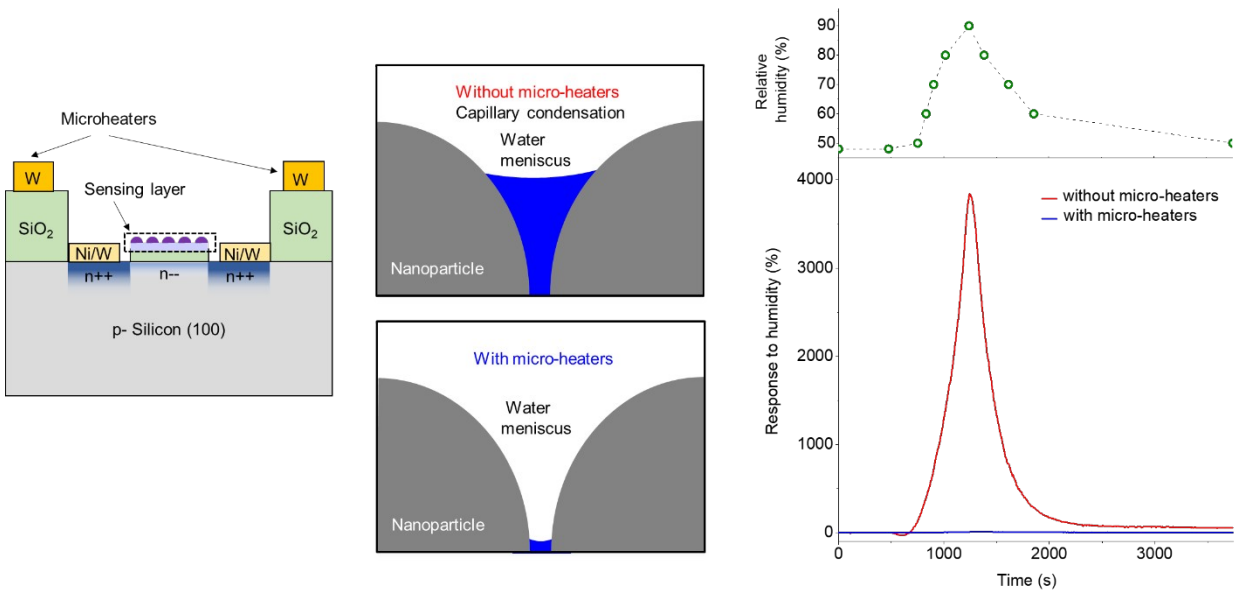
Microheaters
W
W
Sensing layer
SiO2
SiO2
Ni/W
Ni/W
n++
n--
n++
p- Silicon (100)
Without micro-heaters
Capillary condensation
Water
meniscus
Nanoparticle
With micro-heaters
Water
meniscus
Nanoparticle
Relative
humidity (%)
90
80
70
60
50
4000
3000
2000
1000
0
without micro-heaters
with micro-heaters
Response to humidity (%)
0
1000
2000
3000
Time (s)